Air Quality, Atmosphere & Health (2023) 16:881–895
https://doi.org/10.1007/s11869-022-01295-9

Oceanic and atmospheric anomalies associated with extreme precipitation events in China 1983–2020

Y. C. Lee[1] · M. O. Wenig[1] · K. L. Chan[2]

Received: 12 June 2022 / Accepted: 28 November 2022 / Published online: 10 March 2023

Abstract
Observed synoptic anomalies in connection with China's extreme precipitation events/floods in the summers of 1982/83, 1997/98, 2010, 2014, 2015/16, and 2020 are studied. These events mainly occur within the middle and lower Yangtze basins. The dominant moisture source is the Northern Indian Ocean and the Southwestern Pacific Ocean of the Indo-Pacific warm pool (IPWP). Both of these bodies of water have warmed since 1979. In East Asia, the strong land-sea thermal contrast driven by global warming drives the increased East Asian summer monsoon (EASM) circulation, which develops deep convective precipitation. The total precipitable water in the Indo-Pacific region has also been increasing since 1979. The intense southwest Indian monsoon transports moist air to the Yangtze basin in mid-June and forms the Meiyu (plum rain) front. Strengthened Okhotsk/Ural blocking highs in East and West Asia, as well as the Western Pacific subtropical high (WPSH) and the South Asian high (SAH) over south Eurasia, remain stationary for long periods and interact to exacerbate the precipitation. The western edge of the WPSH expands westward towards East Asia to transport moisture. To the north, the WPSH combines with the two blocking highs to trigger more rain. The intensified SAH expands eastward and merges with the extended WPSH to add rain. On the other hand, rainfall is modulated by the El Niño–Southern Oscillation (ENSO), notably in relation to the super El Niño events in 1982–1983, 1997–1998, 2015–2016, and 2020. The research described in this paper highlights changes in the weather systems with warming and, in particular, the enormous and dominating impact of the warming and expanding IPWP on rainfall extremes. Improved seasonal forecasts and planning ahead will protect lives and livelihoods.

Keywords Extreme precipitation 1983–2020 · East Asian monsoon · Indo-Pacific warm pool · Southwest monsoon · Blocking highs · The western Pacific subtropical high · El Niño

Introduction

Extreme climate and precipitation

Extreme climate events have increased in recent decades. These include intense tropical cyclones/hurricanes in East Asia and the Caribbean, serious flooding in South and East Asia, drought in the Indian subcontinent, fires in California/Australia, prolonged heat waves across Europe and America, North Asia, and Australia, a wetter Asian monsoon, ice melting in the Arctic, and glacial melting in Antarctica. The scenario unfolding is that abnormal climate events will intensify.

Significant increases in heavy precipitation and decreases in light precipitation have been reported from widespread regions of the globe. Warming seems to be driving an increase in extremes of rainfall and snowfall across most of the planet, even in arid regions. The heavy precipitation in Asia is apparently triggered by warmer temperatures. This increases the amount of water vapour in the atmosphere, which amplifies warming since water can act as a greenhouse gas. Shimpo et al. (2019) indicated that when the atmospheric temperature increases by 1 °C, the amount of water vapour in the atmosphere increases by approximately 7%. Indeed, most of the warming has occurred within the

✉ M. O. Wenig
mark.wenig@lmu.de

Y. C. Lee
ycleec@netvigator.com

[1] Meteorological Institute, Ludwig-Maximilians-Universität München, Munich, Germany

[2] Rutherford Appleton Laboratory Space, Harwell, Oxford, UK

past 4 decades. Tollefson (2016) indicated that both annual and extreme precipitation increased by 1–2% per decade in dry regions, including western North America, Australia, and parts of Asia.

China's historic floods were considered to be among the Earth's most costly weather-related disasters. Precipitation events in summer account for more than half of the annual precipitation in China, and more than 40% of the summer precipitation occurs during the Meiyu (plum rain) season. A significant increasing trend predominates in the records. Zhang et al. (2008) found an increase in the percentage of heavy rain (defined as rainfall that exceeds 25 mm/day) in the annual rainfall records. Data from meteorological stations in eastern China (1955–2011) were compared with Global Precipitation Climatology Project (GPCP) data (1997–2007) and reanalysis data from various latitude zones. Significant increases in heavy precipitation were found.

Records show that 2020 was the 2nd hottest year on record after 2016 (NOAA 2021). Additionally, the 2020 precipitation event, which began in June, was the worst since 1998 and coincided with one of the coronavirus pandemic years. The Yangtze River received the largest volume of rainfall since 1961, and over 400 rivers rose to dangerous levels. By July 28th of that year, floods had affected 54.8 million people in 27 provinces, autonomous regions, and municipalities. It is widely believed that changes in climate patterns were behind the deadly floods.

The 2016 flood is the fifth most expensive weather-related natural disaster on record outside of the USA, according to the International Disaster Database (Centre for Research on the Epidemiology of Disasters 2017). Rainfall was much heavier that year than it was in 1998, with two main rainfall belts located in the Yangtze River valley and North China. Rainfall was consistently high across the middle and lower Yangtze basins, approximately 140% of the average (NOAA NCEI 2017). The extreme and anomalous rainfall ravaging the Yangtze basin during June and July exceeded 300–400 mm within 10 days, which was ranked as the heaviest 10-day rainfall since 1951. Heavy rain and storms since June 30th caused substantial damage in 11 provinces (Floodlist.com 2016), with 2.9 million people needing to be evacuated. The floods that occurred during July were of historic proportions and were some of the worst since 1998. Intense convection developed over inland Guangdong and moved towards Hong Kong, bringing heavy thunderstorms there.

The flooding disasters of 1998 lasted from the middle of June to the beginning of September. The event was the second worst to hit China in more than 130 years and resulted in a huge loss of life, leaving 14 million people homeless. Compared with 2016, the 1998 disaster had more concentrated rain and wreaked havoc in 24 provinces. Rain events of smaller scales caused floods in Central and Eastern China between June and July 2015, and in South China from April to September 2014. Considerable precipitation was also recorded in the summers of 2013, 2012, and 2010. The study described here focuses on anomalous oceanic and atmospheric circulation systems, including the Indo-Pacific warm pool, which is believed to be strongly associated with the extreme precipitation events that occurred in China from 1983 to 2020.

Data and method

Information regarding the precipitation events that occurred from 2011 to 2019 is drawn from (a) the American Meteorological Society's special report titled "Explaining Extreme Events of (year) from a Climate Perspective" (mainly for the 2016 event) (Herring et al. 2018), which identifies the extreme events and presents assessments of how human-caused climate change may have affected the strength and likelihood of individual events; (b) the US National Oceanic and Atmospheric Administration's (NOAA) Global Climate Report, which provides monthly/annual Climate Briefings and news items; (c) the Bulletin of Flood and Drought Disasters in China 2016, with appendices 3–4 specifically discussing the national droughts and flood statistics that were partially available from the Ministry of Water Resources of the People's Republic of China, 2016. The most serious events are identified. Reports from the media provide retrospective details of the events. For the 2020 event, information is mainly obtained from the media/websites, including floodlist.com.

Extreme events are identified using daily/monthly plots compiled from past records of precipitation rates available from the National Center for Atmospheric Research/National Centers for Environmental Prediction of NOAA (NCAR/NCEP). Daily composites (averages) of the mean precipitation rate and precipitation anomalies, surface outgoing longwave radiation (OLR), geopotential height, zonal and vector wind, specific humidity, and sea surface temperatures and pressures of the reanalysis dataset are plotted and analysed. Time series of sea surface temperatures (also known as surface skin temperature, SST, K, defined as the temperature measured by an infrared radiometer typically operating at wavelengths 3.7–12 μm, NASA 2021) and total precipitable water (kg m^2) up to 2020 are generated for the Indian Ocean and the southwestern Pacific Ocean for selected locations north of Bombay and the Bashi Channel, which are at approximately the same latitude. DataTables and NetCDF files from the NOAA Physical Sciences Laboratory plotting webpage are extracted for the plotting of time series and assorted variables.

Global gridded data are available from 1948 to the present. Long-term means (climatology) are based on those from 1981 to 2010. The NOAA data are derived from the

polar-orbiting environmental satellites of the Joint Polar Satellite System (JPSS) (NOAA 2019). This system includes three polar-orbiting satellites, the Suomi National Polar-orbiting Partnership (Suomi NPP), JPSS-1, and JPSS-2, and consists of five instruments. The JPSS constellation gathers global measurements of atmospheric, terrestrial, and oceanic conditions—including data on atmospheric temperature and moisture, clouds, rainfall, dense fog, fire locations, smoke plumes, sea and land surface temperatures, vegetation, snow and ice cover, and ozone. Short-term, seasonal, and long-term monitoring and forecasting are provided. JPSS satellites orbit the Earth from pole to pole, providing full global coverage twice a day. Polar satellites are the backbone of the global observing system.

Interpolated surface OLR (W/m^2) and composite anomalies were acquired from the NOAA Physical Sciences Division (PSD), which generated the daily OLR dataset. The daily OLR climate data provide radiance observations at a $1.0 \times 1.0°$ resolution. The 500 hPa geopotential height (m) composite anomaly, the composite means and anomalies of the 850 hPa zonal wind (m/s), the 850 hPa vector wind (m/s), and the surface skin temperature (K) were obtained from the NCEP/NCAR Reanalysis dataset.

Results and discussion

Surface precipitation rates/OLR anomalies

The surface precipitation rates (mm/day), which are the average volume of rain, snow, hail, or sleet that falls per unit of area and per unit of time (mm/day), are plotted as composite anomalies for the extreme precipitation days in China, as shown below in Fig. 1, alongside the surface OLR (W/m^2) composite anomaly. Anomalies are departures from the mean. The areas where the most serious rainfall occurred during the extreme precipitation events shown in Fig. 1a, c, e, g, and i are generally well represented by OLR fields (Fig. 1b, d, f, h, j). OLR, a proxy for convective precipitation, is a measure of the amount of infrared energy (watts per square metre) that leaves the Earth's surface and atmosphere and radiates back into space. Areas that radiate less heat than normal indicate more clouds covering the region, as in the cloudy and moist tropics and summer monsoon regions. Troughs of heavy precipitation, therefore, often coincide with areas where the OLR is low.

Oceanic anomalies

The Indo-Pacific warm pool (IPWP)

The IPWP stretches across the western Pacific Ocean and the eastern Indian Ocean and contributes enormous amounts of rain to eastern China. The Yangtze flooding of 2020 has been tied to extreme Indian Ocean conditions (Zhou et al. 2021). It is the largest expanse of the warmest ocean temperatures on Earth. The heat stored within the IPWP advects into the atmosphere, and convection increases atmospheric moisture, which results in extreme rainfall. The warming has been estimated to have increased by up to 1.2 °C compared to the past century (Roxy et al. 2015), which is much more than any other ocean basin and is substantial when compared to a global surface warming of up to 0.8 °C over the same period. During summer, the warm pool in the central-east Indian Ocean has sea surface temperatures greater than 28 °C, the minimum surface water temperature that supports deep convection. Greenhouse gas forcing is the dominant cause of the observed increases in IPWP intensity and size, while the El Niño phase is believed to induce warming in the Indian Ocean warm pool (Pervez and Henebry 2016). The warming is, however, uneven across the region.

This enhanced convection in the central equatorial Indian Ocean causes anomalous easterlies to be strengthened along the equator, resulting in the advection of warm waters towards the western Indian Ocean. The Indian Ocean warm pool, therefore, expands westward. This consistent warming caused the Indian Ocean warm pool to expand twofold between 1981 and 2018 (Roxy et al. 2019). The warming oceans impact atmospheric circulation and the hydrological cycle, which are believed to be associated with increased rainfall over Southeast Asia, northern Australia, Southwest Africa, the Amazon, and even drying over the west coast of the USA. The highest rates of sea-level rise in the ocean have occurred in recent decades. This indicates large increases in ocean heat content, which lead to more active air–sea interactions and has important implications for changes in monsoon rain.

Shifts in the mean state of the tropical ocean could change the relative amounts of expansion in the two adjacent oceans/areas and modulate the impact of changes in the IPWP. A mean state change in this direction, for example, affects the East Asian monsoon by inducing a westward extension of the western Pacific subtropical high (discussed later).

The composite mean SST (K) of the Indian Ocean north of Bombay at 20°N, 70°E, and the Bashi Channel of the Pacific Ocean at 20°N, 122°E, for example, show significant increasing trends during the period from 1979 (according to NOAA data available for that year) to 2020 (Fig. 2a, b, e), with the Pacific portion of the IPWP at a slightly higher temperature. However, the expansion in the Indian Ocean far exceeded that in the Pacific Ocean. Gordon and Fine (1996) suggested that the interocean transport of excess fresh water from the North Pacific Ocean occurs through the Indonesian seas. The Indonesian Archipelago,

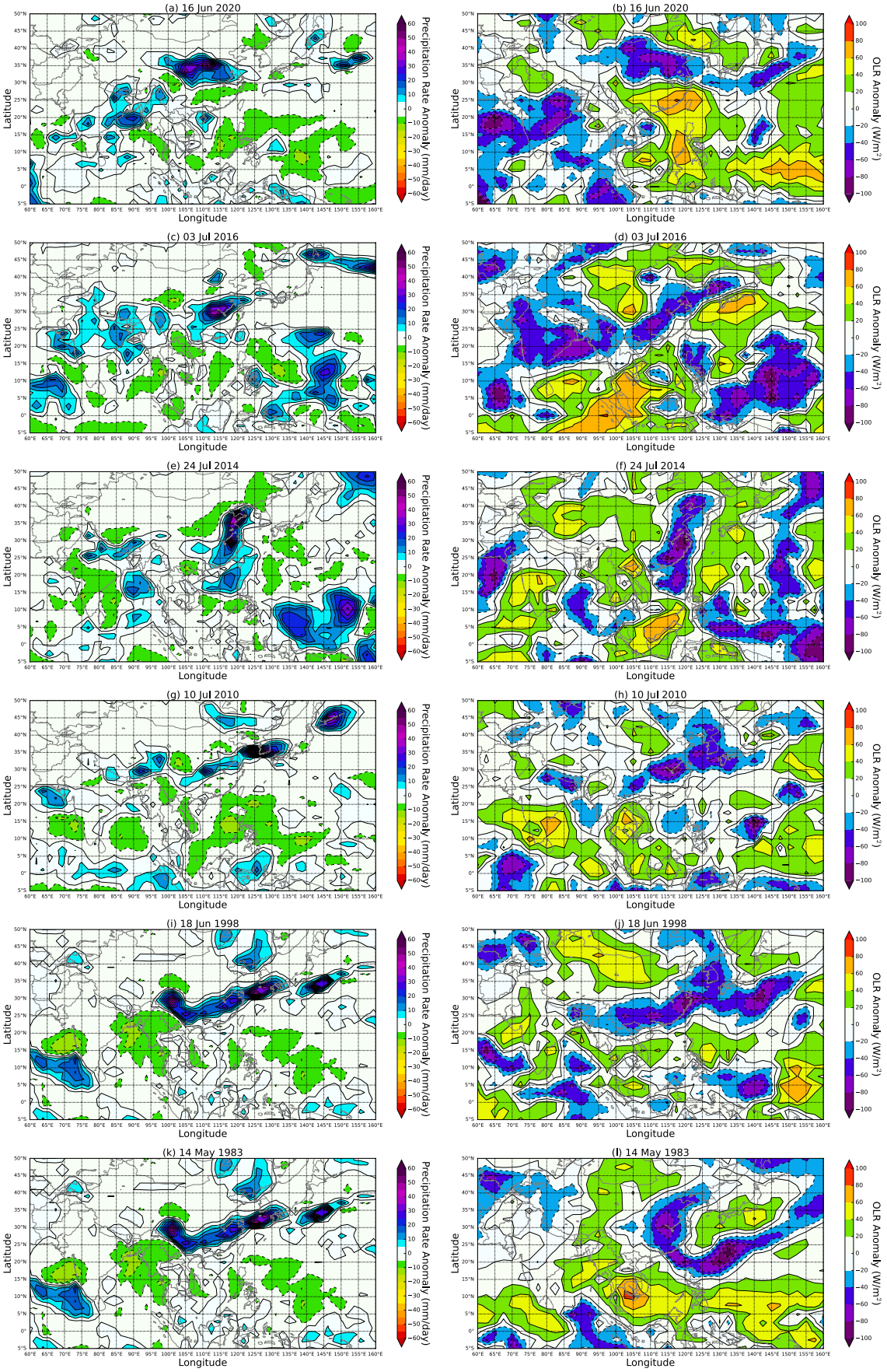
(a) 16 Jun 2020
(b) 16 Jun 2020
(c) 03 Jul 2016
(d) 03 Jul 2016
(e) 24 Jul 2014
(f) 24 Jul 2014
(g) 10 Jul 2010
(h) 10 Jul 2010
(i) 18 Jun 1998
(j) 18 Jun 1998
(k) 14 May 1983
(l) 14 May 1983
Latitude
Longitude
Precipitation Rate Anomaly (mm/day)
OLR Anomaly (W/m²)

◂**Fig. 1** **a**, **c**, **e**, **g**, **i**, **k** Surface precipitation rate (mm/day) composite anomaly for extreme precipitation days (rainfall is not as significant on 10 July 2010) and **b**, **d**, **f**, **h**, **j**, **l** Surface OLR (W/m2) composite anomaly on 16 June 2020, 3 July 2016, 24 July 2014, 10 July 2010, 18 June 1998, and 14 May 1983. High precipitation rates/surface OLR are indicated by blue to purple colour

referred to as the Maritime Continent (~ 10°S–20°N and 90°E–130°E), substantially affects the Pacific and Indian Oceans. The monsoon winds will affect the SST, with southeasterly monsoon winds in boreal summer lowering the SST while the buoyant South China Sea waters in the East Asian winter monsoon period obstruct southward surface water transport in the main strait in the Indonesian seas. The surface layer "freshwater plug" thus formed will inhibit the warm surface water from the Pacific Ocean from flowing southward into the Indian Ocean, leading to a cooler Indian Ocean sea surface, which in turn may weaken the Asian monsoon. Greater warming is found in the West Pacific (Gordon et al. 2003) (see Fig. 2e). On the other hand, the warm and cool SSTs generally agree with El Niño and La Niña conditions, respectively.

The Pacific warm pool is larger and warmer but has less precipitable water than the Indian Ocean (Vinayachandran and Shetye 1991), as shown in Fig. 2c, d, and f. The Indian Ocean pool, however, has seasonal variation in (for example) the surface area of the pool, which contracts by two-thirds from April to September due to interaction with the southwest monsoon. The abundance of atmospheric precipitable water over the southern tropical Indian Ocean contributes to the larger expansion of the Indian Ocean but does not affect the Pacific Ocean.

Excessive moisture from the Northern Indian Ocean

Wang et al.'s (2015) simulations show that the northern Indian Ocean is the dominant oceanic moisture source for precipitation over the Yangtze River valley and southern China in summer. Moist air is carried by monsoons from the Indo-Pacific warm pool. The moist air then crosses the equator near the Somali coastal region and flows towards the Arabian Sea, the Bay of Bengal, and the South China Sea before continuing northward into East Asia (Pan et al. 2017), as shown on 3 July 2016 in Fig. 3b. Their study of the South China Sea shows that only a small volume ($\leq 5.5\%$) of water vapour originates from local evaporation—the bulk is supplied by the northern Indian Ocean and the northwestern Pacific. The South China Sea mainly acts as a water-vapour transport pathway where moisture sources meet. The warming in effect strengthens and deepens the southwesterly winds and provides an increased supply of moisture as the monsoon winds pass over the Indian Ocean.

The El Niño effect

The El Niño–Southern Oscillation (ENSO) causes abrupt changes in weather patterns and is known to be partly responsible for the intense rainfall in China (Sun and Miao 2018). It modulates both Indian and East Asian summer rainfall and contributes to the relationship between Indian and East Asian rainfall variations. Three of the rain episodes coincided with three super El Niño events, which occurred in 1982–83, 1997–98, and 2015–16 in the space of just over 3 decades. With more moisture in the atmosphere, the combination of El Niño and climate change drives rain above past levels. SST and SSP anomalies are closely related to ENSO.

Typical of El Niño and La Niña climate cycles, the sea surface temperatures in the Pacific Ocean along the equator become warmer or cooler than normal at irregular intervals (every 3–6 years). This happened during the years 1983, 1998, 2010, 2016, and 2020. The 2020 La Niña conditions have been in place since August–September 2020, though the La Niña event appeared to have peaked in October–December and was considered a moderate-strength event (World Meteorological Organization 2021). The tropical Pacific Ocean returned to ENSO-neutral conditions during April. Both El Niño and La Niña tend to develop during March–June, reach peak intensity in late autumn or winter, and then weaken in spring or early summer. During La Niña events, cool water drawn up from the depths of the eastern equatorial Pacific strengthens the easterly winds and pushes warm surface water back towards Asia. This occurred in 2020, 2016, 2010, and 1998 (Fig. 3). In the winter of a La Niña year, the unusually strong trade winds blow westward along the equator, and the water pushed west piles up in the West Pacific, creating a warm layer. The thermocline is thus pushed down while it rises in the east. The eastern thermocline allows an increased upwelling with water pulled up by winds from below and brought to the surface, leading to a buildup of cooler-than-normal sea surface temperatures off South America.

The very strong El Niño in 2015–2016 was followed by a weak La Niña. Model and observational analyses showed that the extreme precipitation that occurred in June–July 2016 in the Yangtze basin was strongly correlated with the preceding 2015/16 El Niño conditions (Sun and Miao 2018). 2014 featured a weak El Niño, while (late) 2010 witnessed a relatively strong La Niña (Zhang et al. 2013). A strong SST anomaly related to La Niña conditions was observed in 2010, as shown in Fig. 3c. The 1997–1998 El Niño event began early. By October 1997, this El Niño had already become the strongest in 50 + years. After the classic El Niño pattern fully matured, it evolved into a La Niña event that lasted from mid-June to early September 1998 and exhibited a strong SST anomaly. Wang et al. (2001)

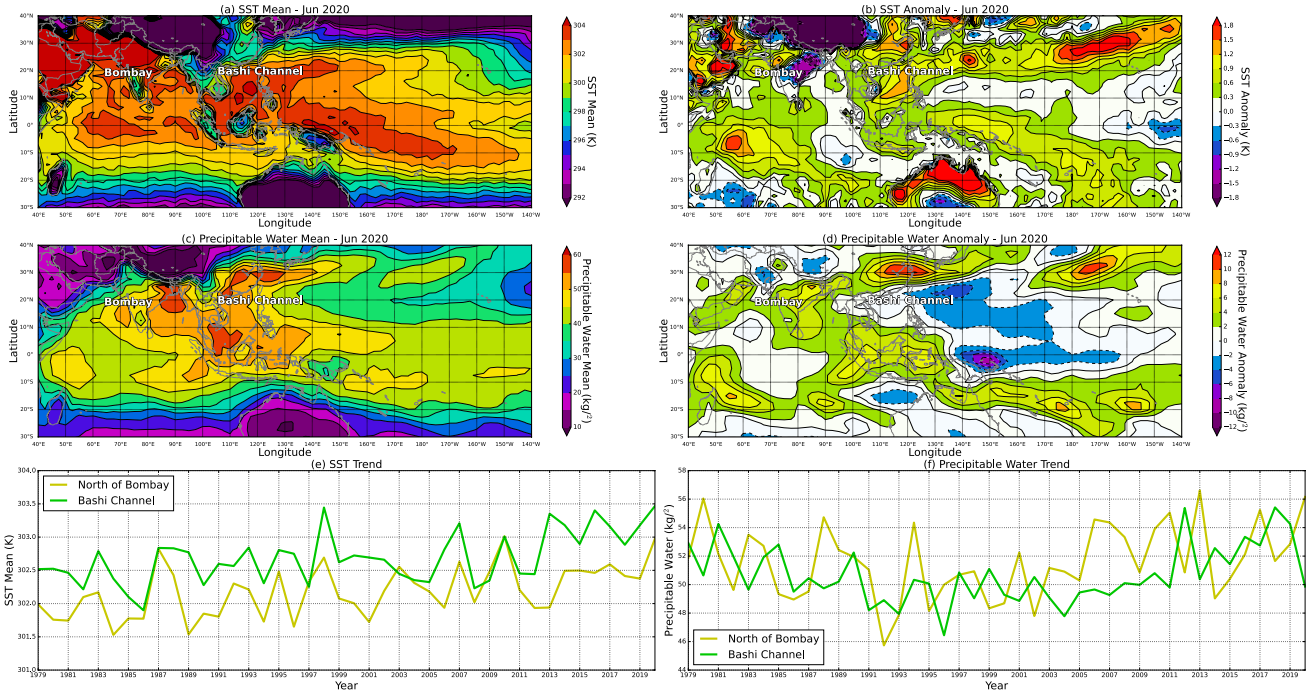

Fig. 2 The Indian Ocean (North of Bombay) and the Pacific Ocean (Bashi Channel). **a**, **b** Surface skin temperature (SST) (°K) composite mean and anomaly June 2020, **c**, **d** precipitable water (kg m.$^{-2}$) composite mean and anomaly June 2020, and **e**, **f** trends of SST and precipitable water for the Indian Ocean and the Pacific Ocean 1979 to 2020

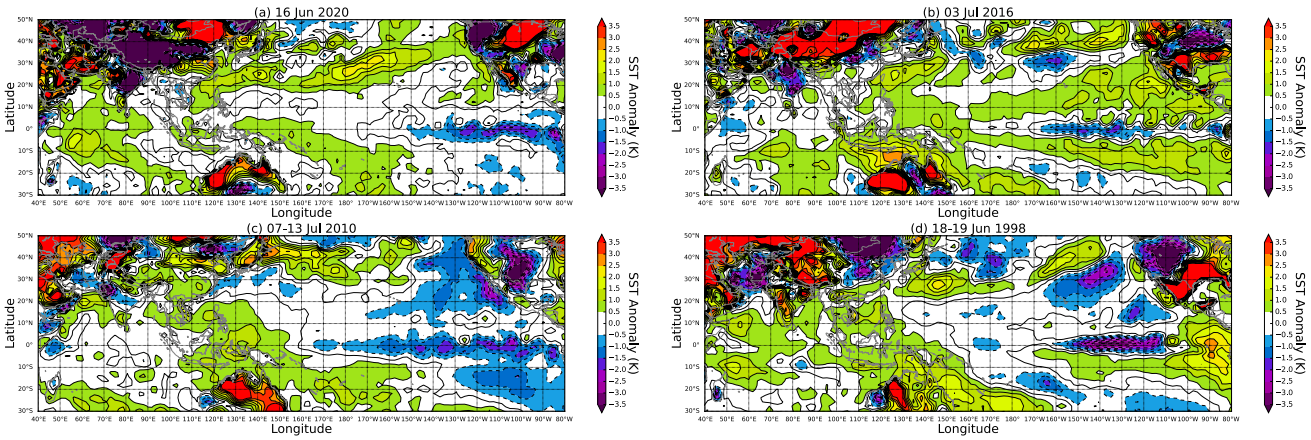

Fig. 3 Surface skin temperature (SST) composite anomaly across the Pacific Ocean on **a** 16 June 2020, **b** 3 July 2016, **c** 7–13 July 2010, and **d** 18–19 June 1998, showing the SST and El Niño/La Niña signals

indicated that the devastating 1998 flood in southern central China may have been partially due to a delayed impact of the 1997/98 El Niño. Observations include a significant positive correlation between the summer SSTs in the NINO-3 region (Niño 3.4 later became favoured for defining El Niño and La Niña events) and 500 hPa geopotential height anomalies over the preceding autumn and winter in subtropical East Asia and the western North Pacific and in northeast Asia. In 1983, an El Niño began to develop in May–September 1982, with the peak El Niño period occurring in the winter between November 1983 to March 1984. The very strong El Niño in 1982–83 was followed by a weak La Niña. It is easier for a La Niña event to last longer (up to 2–3 years) than an El Niño event, which rarely persists for more than a year.

Variations in sea level are good indicators of the presence of an El Niño (see Fig. 4), as seen in 2016, 1998, and 1983. Stronger easterly wind flow increases upwelling,

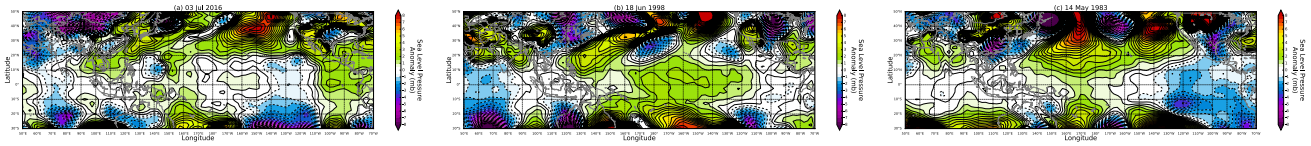

Fig. 4 Sea level pressure (hPa) composite anomaly for **a** 3 July 2016, **b** 18 June 1998, and **c** 14 May 1983, showing negative anomalies in East China and coasts in 1983 and 1998

and a negative sea level anomaly, therefore, reveals the regional extent of anomalous water levels in coastal seas. A sea level anomaly occurs when the 5-month running average of the interannual variation is at least 0.1 m greater than or less than the long-term trend as defined by NOAA's National Ocean Service (NOAA 2018, 2019). The SLP anomaly chart for June 1998 (Fig. 4b) shows that negative anomalies extended from the lower Yangtze to as far north as Japan. During an El Niño, the sea level in the eastern Pacific is sufficiently above average, whereas an increase in sinking air over the western Pacific leads to higher surface pressure. SLP anomaly charts clearly show negative anomalies in East China and along the coasts in 1983 and 1998 (Fig. 4c and b). In South China, a monthly sea level anomaly was recorded in Hong Kong (at North Point/Quarry Bay) in October and November of the extreme El Niño years 1997 and 1982 (Hong Kong Observatory 1999).

The SST and SSP that coincided with the precipitation episodes in China, which are El Niño/La Niña related, are shown in Fig. 2. The direct atmospheric response to the Pacific SST pattern is a large-scale circulation anomaly in the lower troposphere that occupies the entire northern North Pacific (as described in Strong East Asian summer monsoon (EASM) Section on the East Asian summer monsoon). The El Niña signal is clearly evident in the westward-moving anomalous current observed in the tropical Western and Central Pacific in Fig. 3a to d for four of the episodes, whereas the 1982/83 El Niño featured a pronounced eastward expansion of the West Pacific warm pool.

Previous studies have shown that El Niño can affect East Asian summer monsoon rainfall via atmospheric teleconnections. The WPSH bridges the El Niño events and the East Asian summer monsoon. Wang et al. (2017) suggested that during strong El Niño events, the WPSH is coupled with a pronounced anomalous SST dipole, cooling to its east and southeast in the western North Pacific and warming to its west and northwest over the East Asian Seas and the northern Indian Ocean from the El Niño developing autumn to the decaying summer. The coupling provides positive feedback between the WPSH and the underlying SST dipole anomaly, which amplifies the WPSH from fall to spring and maintains it into the summer, where El Niño decays. The El Niño impacts can be significantly amplified and prolonged during the decaying phase of strong El Niño events.

Atmospheric anomalies

Global warming plays a pivotal role in driving synoptic meteorological anomalies that give rise to extreme rain. Along with a long-term trend of surface air temperature increase due to warming, there is a markedly increasing trend in the amount of water vapour in the air, as shown in Fig. 2c, d, and f. When the atmospheric temperature increases by 1 °C, the amount of water vapour in the atmosphere increases by approximately 7% (Shimpo et al. 2019). Very intensive air–sea interaction takes place in the oceans.

Strong East Asian summer monsoon (EASM)

The EASM is the dominant mode over East Asia in summer and delivers enormous amounts of precipitation with pre- and post-monsoon-onset events. It connects the configurations of the Meiyu trough, a persistent stationary front, the WPSH, and the midlatitude highs.

The onset of Meiyu is preceded by an increase in convective activity, both in extent and intensity, in the East Indian Ocean and the Bay of Bengal. The rainy season in spring usually first appears over South China and the East China Sea from late March to early May. Deep convection (i.e., convection to great depths of the atmosphere, as illustrated by the depth of colour of the OLR) develops northward of the Bay of Bengal, south China, and along the eastern coast of China, as shown in Fig. 1b, which depicts 16 June 2020. A shallow humid southwesterly wind moves across the southern parts in April. This is followed by south-to-southeasterly winds bringing rainfall as a Meiyu front, which lasts for nearly 2 months. The record-breaking Meiyu in the Yangtze-Huaihe River valley in 2020 was characterised by early onset, delayed retreat, long duration, and wide meridional rain belt (Ding et al. 2021). Later, the sequential passages of the Meiyu rainband shift to the north and east, into South Korea and Japan from June to July, and into eastern

China from July to August. The rainband eventually dissipates, and the rainy season ends during the summer when the warm air mass associated with the subtropical ridge (WPSH) becomes strong enough to push this front to the north of the region and away.

Wang et al. (2019) found that the annual mean sea surface temperatures increased at a rate of 0.21 ± 0.08 °C per decade over the East China Sea, but the land has warmed even more, with global surface warming of up to 0.8 °C (Roxy et al. 2015). The anomalous surface warming over the land relative to the ocean induces a land–sea thermal and geopotential height contrast throughout the troposphere (Kamae et al. 2014). The strong land-sea thermal contrast in the lower troposphere drives the increased EASM circulation. A front forms when the warm moist air over the Pacific advances over the cooler continental air mass. The 500 hPa geopotential height (Z500), which is closely associated with precipitation, has actually risen during the last few decades (Xoplaki et al. 2000). A significant global increase in the annual and seasonal mean geopotential height due to human influence was confirmed by reanalysis datasets. The Asian summer monsoon in the summers of extreme rainfall appeared abnormally strong in the lower to mid-troposphere, while the thermal contrast in the upper troposphere was almost unchanged by warming. According to Ding and Chan (2005), in addition to the Pacific and the Indian Ocean Sea Surface Temperatures (SST), the snow cover in Eurasia and on the Tibetan Plateau is believed to also contribute to and affect the activity of the East Asian summer monsoon.

Hence, on extreme precipitation days (as shown in Fig. 3a to d), an SST front is observed over the East China Sea. An east−west zone of disturbed weather along the front stretches along the East China coast from May to June, characterised by strong convective precipitation embedded in the wide cloud zone (as shown in the OLR areas in Fig. 1). A very significant anomaly of precipitable water is found in Central China in June 2020 (Fig. 2d). The lower- to mid-tropospheric air, therefore, contains large amounts of water vapour. Apparently, deep convection anomalies follow the SST anomalies. The turbulent mixing of deep convection moves air from the lower to the upper atmosphere as upward motion is strengthened. The rate of occurrence of deep cumulus convection along the rainband reveals the extent of the enhancement. Regionally, Matsumura et al. (2015) indicated that East Asian convective activity has moved northward and enhanced over the past 3 decades. The northward movement appears obvious for the June 2020 rainfall episode.

When the East Asia summer monsoon moves from South China to the Yangtze basin in mid-June, the Indian summer monsoon sets in at nearly the same time over the Indian Peninsula. Therefore, the onset of the Indian rainy season and the Meiyu are synchronised in early to mid-June, which greatly enhances the moisture supply from the Bay of Bengal and the South China Sea. The monsoon systems occasionally interact with each other.

Intense Southwest Monsoon

As a result of global warming, monsoons are altered and become more irregular, especially with the Southwest monsoon. Li et al. (2008) proposed that near the surface, the Indian Ocean warming forces an anticyclonic anomaly over the subtropical western Pacific and intensifies the southwesterly winds to East China. The tropical Pacific winds have purportedly (Luo et al. 2012) strengthened in the past 2 decades, and the enhanced Indian Ocean warming favours stronger trade winds in the western Pacific via the atmosphere through the Pacific Ocean–atmosphere interactions. Model simulations suggest that the warming of the Indian Ocean relative to the Pacific could play an important role in modulating Pacific climate changes.

The OLR composite anomalies shown in Fig. 1d and j indicate strong monsoon activity around India during the heavy precipitation events in 1998 and 2016, which is well represented by wide areas of purple-coloured negative OLR anomalies. The extent and overall activity of the monsoon circulation and rainfall are shown. Abnormalities are clearly observed in the warmed-up northern Indian Ocean and the western Pacific. Intense rainfall clouds coincide with the negative OLR anomaly and indicate deep convection, as explained earlier in the "Strong East Asian summer monsoon (EASM)" section.

The interplay between atmospheric winds and ocean waters south of India has a major influence on the strength and timing of the Indian monsoon (MIT 2019). The warm Indian subcontinent induces strong winds to sweep across the Indian Ocean and up over the South Asian landmass. The stronger this interplay, or coupling between winds and ocean, the larger the difference between land and sea temperature, and the stronger the intensity of the monsoon. The Himalayas are believed to have insulated the Indian subcontinent, thus enhancing the summer land/ocean temperature difference. By studying the barium-calcium signature of dust present in Red Sea corals, Bryan et al. (2019) found that over the past 250 years, the summer South Asian monsoon circulation has evolved with the warming climate, revealing a multi-century-long monsoon intensification, with decreased multidecadal variance.

The transport path of moisture is well illustrated by the positive zonal southwesterly wind anomalies (a component of wind along a particular parallel of latitude) at 850 hPa. The upper air feature's geopotential height approximates the actual height of a pressure surface above the mean sea level at which the observation was taken. The temperature

at 850 hPa is approximately 1.5 km above sea level, usually just above the boundary layer, and is used to show frontal zones and distinguish between warm and cold air masses. The diurnal (daily) cycle in temperature at this level is generally negligible. The East Asian monsoon carries moist air, mostly from the northern part of the Indian Ocean and the Pacific Ocean, to East Asia, as described above, and over the Yangtze River valley and south China in summer, as shown in Fig. 5. Positive wind anomalies are prominently observed on all days during precipitation episodes. Such circulation anomalies have been suggested to be normally expected during El Niño events (Lai et al. 2015). The prominent positive colours on the charts shown in Fig. 5 for 16 June 2020, 3 July 2016, and 18 June 1998 illustrate the strong zonal flow observed in strong El Niño years.

According to Sree Raghav and Mrudula (2016), horizontal transport of moisture occurs in the lower atmosphere in an atmospheric/tropospheric river, which is a narrow corridor of concentrated moisture from tropical regions towards the poles across the mid-latitudes. Such high-intensity transport is found to occur during the pre-monsoon and monsoon periods (JJA) (and the El Niño phase).

Atmospheric anomalies causing persistent rain

Blocking high-pressure systems In addition to the Meiyu trough, the circulation pattern of the Asiatic monsoons features dominant high-pressure systems, which include the midlatitude Okhotsk and Ural blocking highs, the WPSH, and the SAH.

The distribution of anomalies in the circulations is indicated by plots at the 100, 500, and 850 hPa geopotential height levels, approximating the actual height of a pressure surface above the mean sea level. Cold air causes pressure surfaces to be lower within air masses, while warmer air allows the pressure surfaces to be higher. Geopotential height anomalies at the 500 hPa pressure level (approximately 5.5 km above sea level) depict synoptic circulation changes. High heights reveal ridges such as subtropical ridges and anticyclones (Fig. 5), while lower heights appear as troughs and are often associated with cloudy conditions and precipitation. The pressure systems and their anomalies are examined during each episode day. Anomalies relating to the East Asian monsoon and the southwesterly monsoon are clearly illustrated by geopotential heights.

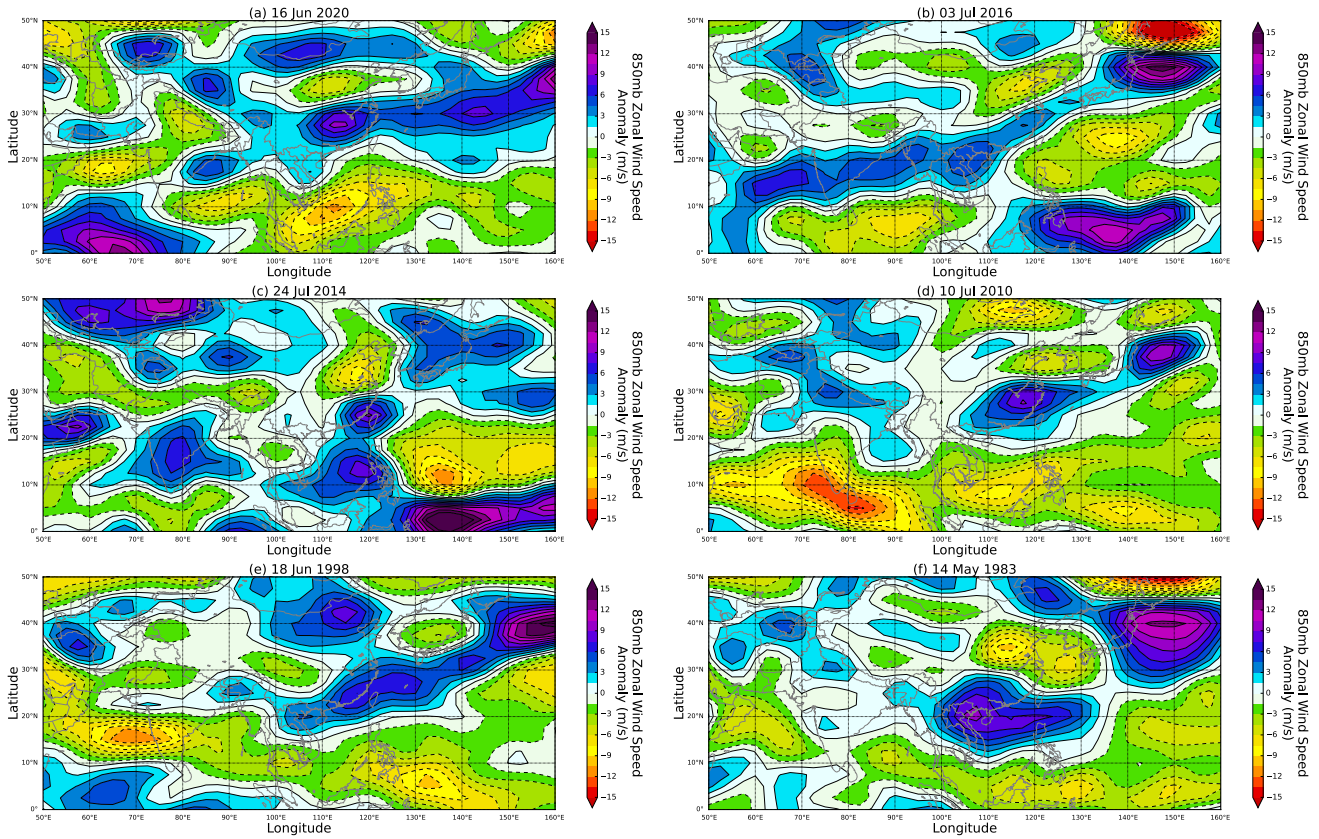

Fig. 5 A 850 hPa zonal wind (m/s) with positive anomalies from India and the neighbouring seas to South and Eastern China on **a** 16 June 2020, **b** 3 July 2016, **c** 24 July 2014, **d** 10 July 2010, **e** 18 June 1998, and **f** 14 May 1983

A blocking high blocks the passage of weather systems and is one of the most important weather patterns in mid- and high latitudes. In Asia, it consists of the Okhotsk high, a negative geopotential height anomaly centred in Northeast China over the sea of Okhotsk, and the Ural High, another negative centre near the Ural Mountains in west Asia, with a trough, a positive centre between the two, near Lake Baikal. The development of the Okhotsk high in Japan (south of the Okhotsk Sea) during the heavy rain of 2018 was caused by the significant and persistent meandering of the polar front jet stream (Shimpo et al. 2019) and the subsequent development of a stationary high-pressure system over eastern Siberia.

A single blocking high typically lies to the south of Lake Baikal with blocking high accompanied by a deep trough to its east and extends into the southern Yangtze. This is, however, not found during the precipitation episodes. A typical circulation pattern in the Meiyu season involves a low-pressure system over Lake Baikal that develops between two high-pressure systems to the east and west. Double blocking is more frequent in summer. The anomalous Ural High over West Asia has been suggested to be partly forced by anomalous Indian Ocean heating.

The relative strengths of the Ural and Okhotsk highs (Fig. 6) vary with events. Their relatively continuous and stable pattern affects the intensity, duration, and frequency of rain. The establishment of strong and stable high-latitude double-blocking highs is beneficial to maintaining a relatively stable state of the WPSH and strengthening its westward extension. The double-blocking highs determine the rainfall distribution and strong precipitation areas during the Meiyu season (Wu 2002). A significant protracted positive anomaly occurred over the Ural in the summers of 2014, 2010, and 1998 (Fig. 6), while abnormal convections occurred over the tropics. During May–July 2016, the Ural High was weaker than normal, while the blocking high over the Okhotsk Sea was strong. In 1998, the Okhotsk high was particularly strong despite a weakening of the summer Okhotsk high over the past 3 decades with a decrease in sea level pressure (SLP) (Matsumura et al. 2015). The Sea of Okhotsk is sensitive to global warming, which has been greatest on the southern boundary of the polar region near the Sea of Okhotsk (Kamae et al. 2014). According to Matsumura et al. (2016), the northward shift of the East Asian rainband over the Northwest Pacific contributes to the weakening of the Okhotsk high and intensification of the WPSH. This is despite the fact that double blocking has generally intensified in recent decades (Liu et al. 2017).

The blocking highs extend and continuously steer cold/dry air from mid to high latitudes to the Yangtze Valley, where it encounters warm/moist air from lower latitudes conveyed by intensified southeasterlies. These southeasterlies are associated with a westward shift of the WPSH. A front is formed, which leads to spells of anomalous torrential rain. The intensity of the blocking highs and the WPSH have been considered two key factors that determine the Yangtze Valley and South China's rainfall patterns and the intensity of the precipitation (Liu et al. 2017).

Other atmospheric anomalies contributing to rain

The intensified West Pacific Subtropical High (WPSH) The WPSH is a semipermanent, high-pressure system at 500 hPa in the lower troposphere over the Western Pacific Ocean. It has intensified during the past 3 decades (Matsumura et al. 2015; Choi and Kim 2019) in summer with increases in sea level pressure and geopotential height. The westward expansion of a strong WPSH to the western North Pacific is generally attributed to the intense warming of the Indian Ocean. However, its expansion near Japan is associated more with the persistent northward meandering of the subtropical jet stream in the upper troposphere (Shimpo et al. 2019).

According to the extent to which the WPSH expands towards the East China Sea, extremely moist air will flow in the lower troposphere over East Asia. In 2020, 2016, 1997/1998, and 1982/1983 El Niño events, abnormal westward extensions of the subtropical high were clearly observed (Fig. 6). During the 3 July 2016 episode, the WPSH extended as far west as the northern Bay of Bengal. One of the important reasons why the WPSH during May to July 2016 was relatively stronger than in 1998 is that the Indian Ocean warming mode was particularly strong in 2016. The WPSH is substantially influenced by sea surface temperature (SST) variations in the tropical Pacific and Indian Oceans. The WPSH is clearly reinforced due to global warming (Choi and Kim 2019). As discussed in "The El Niño effect" Section, the anomalous WPSH and Indo-Pacific SST dipole indicate that the composite anomalies are linked with strong El Niño events.

The westward extension causes moisture to be transported by the southwesterly winds at the western edge of the strong WPSH to feed the Meiyu front. This, along with the strengthening of the Siberian high and the monsoon low, results in moisture transfer in an upward motion and the appearance of a thermal gradient along the Meiyu front. According to Guan et al. (2019), the low-level jet along the northwestern edge of the WPSH simultaneously transfers a large amount of water vapour into East Asia. Strengthened by the blocking highs, the WPSH triggers excessive precipitation in the Yangtze River Basin. Typically, the strong and steady double-blocking highs maintain a relatively stable WPSH, which cannot progress northward when the Okhotsk high is active. Under stable atmospheric pressure conditions, the continuous confluence of warm vapour from the south and cold air from the north additionally brings large amounts of rain to the Yangtze Valley. The position and intensity of the subtropical high, such as

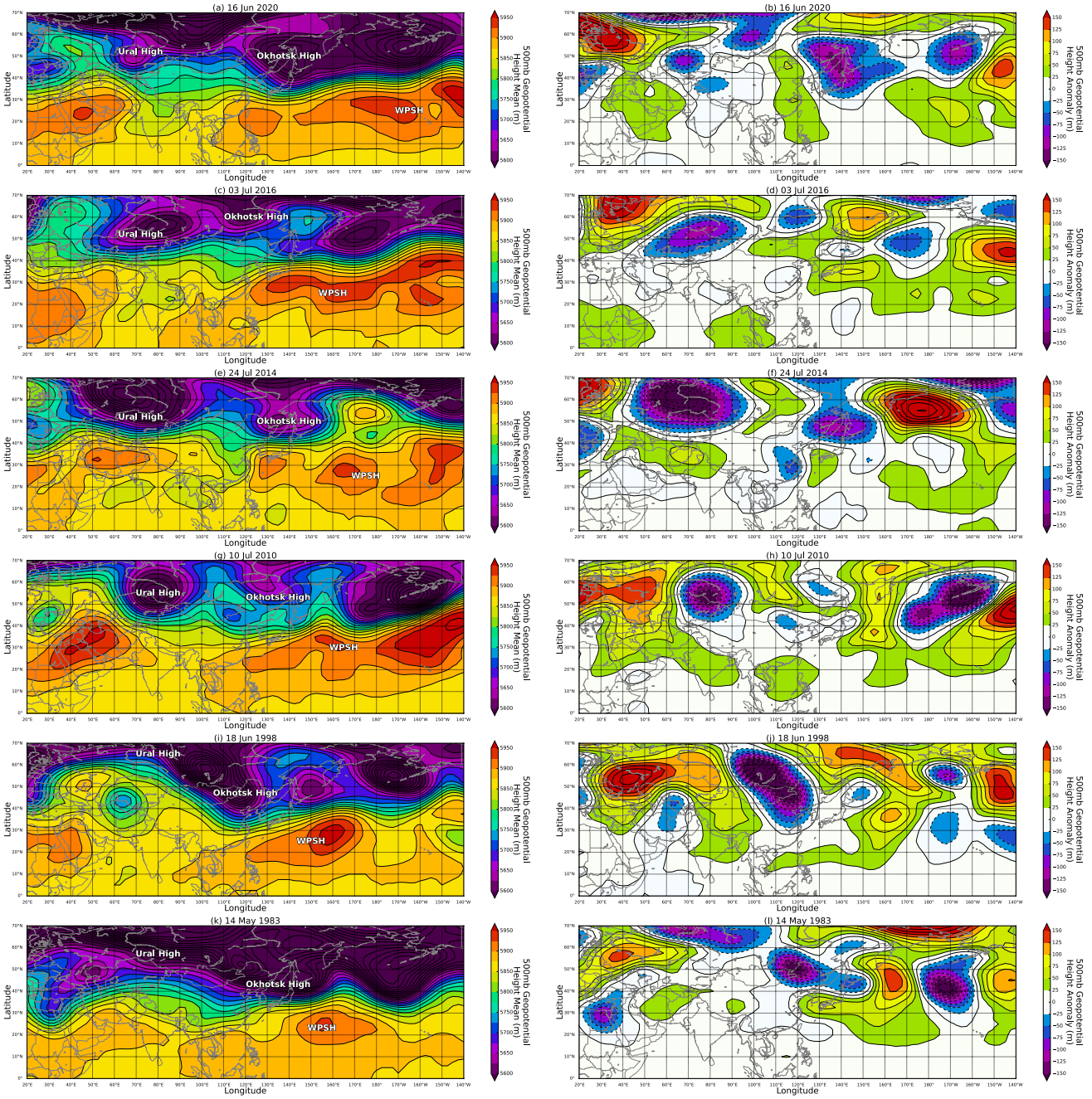

Fig. 6 A 500 hPa geopotential height composite mean (**a**, **c**, **e**, **g**, **i**) and anomaly (**b**, **d**, **f**, **h**, **j**) on 16 July 2020, 3 July 2016, 24 July 2014, 10 July 2010, 18–19 June 1998, and 14 May 1983, showing locations of the Okhotsk and Ural highs, and the West Pacific subtropical high

the blocking highs, therefore play a critical role in the position of the summer rain belt in China.

Among all the heavy precipitation days listed in this paper, the Indian Ocean warming in 2016 (and 2020) was among the greatest, which, as mentioned earlier, was one of the important reasons for the relatively stronger WPSH in 2016. The intensity of the high-pressure Okhotsk, Ural, and WPSH systems was believed to have increased during the second half of the twentieth century. According to Choi and Kim (2019), the combination of global warming and the El Niño effect seems to have significantly influenced the location and intensity of the WPSH, which is said to bridge El Niño events and the East Asian summer monsoon.

The South Asian High (Tibetan High) The SAH is a high-pressure system at 100 hPa in the upper troposphere over the southern part of the Eurasian continent, covering both

the subtropics and midlatitudes. It forms as a result of the sensible heat flux over the Tibetan Plateau and South Asian monsoon precipitation. It is a warm centre found near the Tibetan Plateau in summer. Models (Zhang et al. 2017) suggest that under global warming, the latent heating change over the regions out of South Asia, the Indian Ocean, and the western Pacific leads to a northward shift of the SAH, as observed during the extreme precipitation days examined in this study.

Rain is concentrated in elongated (Fig. 7) rain belts that stretch to China, Japan, and Korea (Qu and Huang 2016).

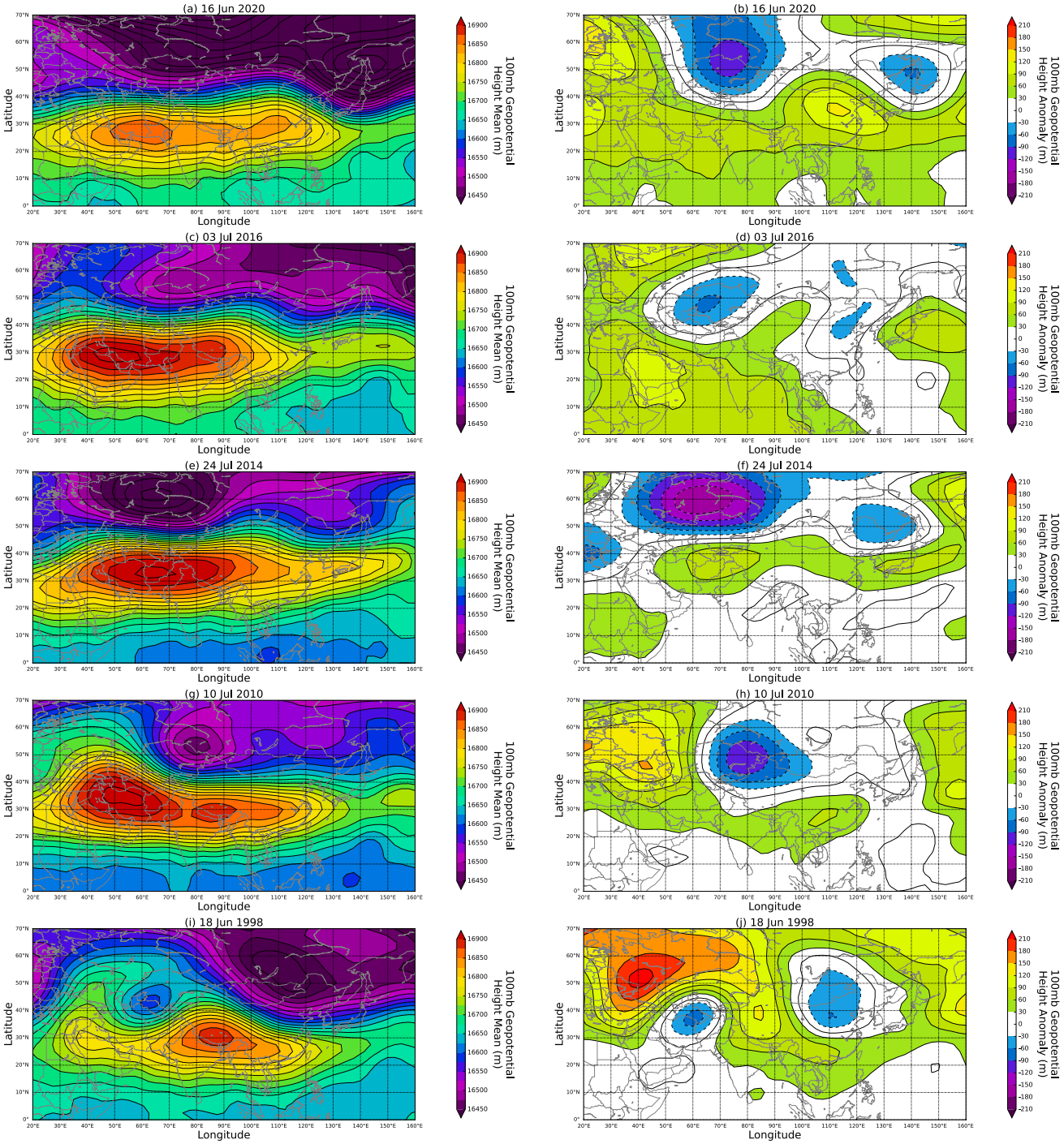

Fig. 7 **a**, **c**, **e**, **g**, **i** A 100 hPa geopotential height composite mean and **b**, **d**, **f**, **h**, **j** anomaly for 16 June 2020, 3 July 2016, 24 July 2014, 10 July 2010, and 18 June 1998, showing the South Asian high (SAH)

An intensified SAH leads to a strengthened southwestwardly located WPSH and indirectly influences the position of the rain belt in China in summer. The SAH is located in the southern part of Indochina before the onset of the South China summer monsoon. It then moves towards the northwest and significantly intensifies with convective activity. The northwest−southeast movement and magnitude of the SAH influence the summer precipitation across eastern China (Ning et al. 2017). When the SAH is located anomalously northwest, more extreme precipitation occurs over the northern part of eastern China.

When the intensified SAH expands eastward during days of extreme rainfall, it encounters an enhanced westward-extended WPSH (Choi et al. 2016). The merging of warm and cold advection enhances water vapour transportation over the Yangtze River Basin. The anomaly was prominent on 24 July 2014 and 18 June 1998 (as shown in Fig. 7). The resulting precipitation, in turn, induces anomalous southeasterly winds. The narrow meridional scale of the SAH obviously makes the rainfall less concentrated than in South Asia. The positive geopotential anomalies over Central Asia induce the deep barotropic Korean High (Ning et al. 2017), which increases convergence over the northern part of eastern China at the northwestern edge of the Korean High. Thus, more water vapour is transported to eastern China.

The centre of the SAH shifts between the Iranian Plateau to the west or the Tibetan Plateau to the east (its two preferred locations) (Wei et al. 2014). The centre of the SAH was over the Iranian Plateau and was extending eastward to the Tibetan Plateau on most of the extreme precipitation days (Fig. 7) (except 14 May 1983, when the SAH was still in the formative stage in spring) (Liu et al. 2013). In contrast, the SAH was conspicuously strong on the Tibetan Plateau in 1998. The mean seasonal cycle of the SAH and its centre is found (Nützel et al. 2016) to be dominated by the expansion of convection in the South Asian region on the southeastern border of the SAH.

Conclusions

Extreme precipitation in China has increased in recent decades. The most serious events that occurred during the 1983–2020 study period are analysed in this work in the context of observed oceanic and atmospheric anomalies, including the role of a warming IPWP, stronger monsoons and blocking by mid-latitude high-pressure systems. The daily composite (averages) precipitation rates (mm/day) and mean anomalies on (i)16 June 2020, (ii) 3 July 2016, (iii) 24 July 2014, (iv) 10 July 2010, (v) 18 June 1998, and (vi) 14 May 1983 are ascertained by the interpolated surface the outgoing longwave radiation (OLR, W/m^2) anomaly. The East Asian monsoon is directly associated with the warming Indo-Pacific warm pool (above 28 °C) between the western Pacific Ocean and the eastern Indian Ocean. The northern Indian Ocean is the dominant source of moisture transported by strong southwesterly monsoon winds to East Asia.

Comparisons are made between two approximately parallel locations: north of Bombay at 20°N, 70°E, and the Bashi Channel in the Pacific Ocean at 20°N, 122°E, during the period from 1979 to 2020. With the world's highest rates of sea-level rise in recent decades, the ocean heat content of the Indian Ocean has substantially increased. The Pacific warm pool is, however, even warmer but has less precipitable water than the Indian Ocean. In short, both the composite mean surface skin temperature (SST, K) and the composite mean precipitable water (kg m^{-2}) over the Indian and Western Pacific Oceans significantly increased from 1979 to 2020.

Anomalous surface warming over the land in eastern China is clearly shown by the geopotential heights. Warming induces a land–sea thermal contrast, especially in the lower to mid-troposphere, which drives the increased EASM circulation. On extreme precipitation days, a strong SST front is observed over the East China Sea. This front is an east−west wide cloud zone of disturbed weather with strong convective precipitation embedded and forms when the warm moist air over the Pacific advances over the cooler continental air mass. The anomalous deep convections reach great depths and tend to follow the SST anomalies. A Meiyu (plum rain) front is accompanied by moist southwesterlies from the Indian Ocean, which have been strengthened and deepened by warming. When the East Asian summer monsoon moves from South China to the Yangtze basin in mid-June, the Indian summer monsoon sets in nearly synchronously over the Indian Peninsula. The east−west wide cloud zone later shifts northwards and finally moves to South Korea and Japan. The rainy season ends during summer when the warm air mass of the WPSH becomes strong enough to push the front north of the region.

In addition to their relationship with monsoons, SST and pressure SLP are closely linked to El Niño and La Niña. Some of the extreme precipitation events occurred simultaneously with the three "super El Niño events" in 1982–1983, 1997–1998, and 2015–2016. The extreme precipitation that occurred in the summer of 2016 and during the 1998 and 1983 episodes was in fact strongly correlated with the preceding El Niño conditions and believed to be a delayed impact.

Blocking by high-pressure systems across Asia exacerbates rainfall. The location of the West Pacific Subtropical High and the intensity of the double blocking highs—the Okhotsk and the Ural highs—are key factors that determine the Yangtze and South China rainfall patterns. Strong double-blocking highs are observed on all extreme precipitation days in this study. The confluence of cold and warm air masses results in long periods of rain. The double-blocking

highs strengthen and stabilise the westward-extended WPSH, causing persistent rain.

The southwestward expansion of the WPSH in 2020, 2016, 1997/1998, and 1982/1983 El Niño events led to significant warming in southern China due to strong downward air motion. Water vapour flux is thereby increased and greatly benefits the Meiyu regimes. The WPSH is perceived to couple El Niño events with the East Asian monsoon. The WPSH was significantly influenced by the SAH during the 18 June 1998 and 3 July 2016 episodes, during which an eastward expansion of cold SAH air converged with an enhanced and westward extended WPSH that increased the water vapour transport.

The extensive summer Asian monsoon anomalies that are associated with extreme precipitation suggest that a changing monsoon is prevailing. Rainfall has become irregular and highly anomalous, and flooding has increased. The monsoon is a vital part of life in East Asia and other monsoon areas of the world. Close to half of the global population depends on monsoon rainfall. Therefore, an in-depth and holistic understanding of the factors contributing to episodic monsoon events in all monsoon areas of the world is crucial for devising long-term multi-pronged plans of action, especially in the context of strengthening the global response to climate warming. With improved seasonal forecasts, planning ahead will protect lives and livelihoods.

Acknowledgements The authors would like to thank the US National and Oceanic and Atmospheric Administration (NOAA)'s Earth System Research Laboratory (ESRL) and Air Resources Laboratory (ARL) for the provision of meteorological data and analysis tools for their analysis. Thanks are also due to the Hong Kong Observatory for providing local data.

Author contribution Mark Wenig (the second author) manages the study as the supervisor for the work, including conceptualising and deciding on the scope of work, editing, reviewing the research materials, and overall supervision. Y.C. Lee (the first author) investigates, collects data, analyses, and interprets results, reviews references, and drafts the main parts of the paper. K.L. Chan (the third author) participates in the editing and reviewing and also provides most of the graphical input. All authors read and approved the final manuscript.

Data availability Sources of the data supporting the results reported in the article are provided in respective parts of the article. The datasets used and/or analysed during the current study are available from the corresponding author on request.

Declarations

Ethics approval There are no ethical issues relevant to the study.

Consent to participate The study does not involve human subjects.

Consent for publication The study does not involve human subjects.

Competing interests The authors declare no competing interests.

References

Bryan SP, Hughen KA, Karnauskas KB, Farrar JT (2019) Two hundred fifty years of reconstructed South Asian summer monsoon intensity and decadal-scale variability. Geophys Res Lett 46(7):3927–3935

Centre for Research on the Epidemiology of Disasters (CRED) Institute of Health and Society (IRSS) Université catholique de Louvain – Brussels, Belgium (2017). Debarati Guha-Sapir, Philippe Hoyois, Pascaline Wallemacq and Regina Below: Annual disaster statistical review 2016 the numbers and trends

Choi W, Kim K (2019) Summertime variability of the western North Pacific subtropical high and its synoptic influences on the East Asian weather. Sci Rep 9:7865. https://doi.org/10.1038/s41598-019-44414-w

Choi K, Kim B, Zhang R, Nam J, Park K, Kim J, Kim D (2016) Possible influence of South Asian high on summer rainfall variability in Korea. Clim Dyn 46:833–846. https://doi.org/10.1007/s00382-015-2615-0

Zhang DQ, Feng GL, Hu JG (2008) Trend of extreme precipitation events over China in last 40 years Chin. Phys Soc and IOP Publishing Ltd Chin. Phys B, Vol 17(2)

Ding, Y, Chan, J. The East Asian summer monsoon: an overview. Meteorol. Atmos. Phys. 89, 117–142 (2005). https://doi.org/10.1007/s00703-005-0125-z

Ding Y, Liu Y, Hu ZZ (2021) The record-breaking Meiyu in 202 and associated atmospheric circulation and tropical SST anomalies. Adv Atmos Sci. 6:1–14. https://doi.org/10.1007/s00376-021-0361-2

Floodlist.com retrieved July 2018 from: http://floodlist.com/asia/china-floods-yangtze-river-july-2016. Accessed 20 May 2019

Gordon AL, Fine R (1996) Pathways of water between the Pacific and Indian oceans in the Indonesian seas. Nature 379:146–149

Gordon A, Susanto R, Vranes K (2003) Cool Indonesian throughflow as a consequence of restricted surface layer flow. Nature 425:824–828. https://doi.org/10.1038/nature02038)

Guan W, Hu H, Ren X, Yang X-Q (2019) Subseasonal zonal variability of the western Pacific subtropical high in summer: climate impacts and underlying mechanisms. Clim Dyn 53:3325–3344. https://doi.org/10.1007/s00382-019-04705-4

Herring SC, Christidis N, Hoell A, Kossin JP, Schreck III CJ, Stott PA Eds. (2018) Explaining extreme events of 2016 from a climate perspective. Bull Amer Meteor Soc, 99(1), S1–S157

Hong Kong Observatory Reprint 310 (1999) Some impacts of El Niño and La Niña events on the weather of Hong Kong. Chang WL, Workshop on the impact of the El Niño Southern Oscillation (ENSO) / La Niña on meteorology and hydrology in the Typhoon Committee Area, Macau, 29 June–1 July 1999

Kamae Y, Watanabe M, Kimoto M (2014) Shioga H (2014) Summertime land–sea thermal contrast and atmospheric circulation over East Asia in a warming climate—Part I: Past changes and future projections. Clim Dyn 43:2553–2568. https://doi.org/10.1007/s00382-014-2073-0

Lai AWC, Herzog M, Graf HF (2015) Two key parameters for the El Niño continuum: zonal wind anomalies and Western Pacific subsurface potential temperature. Clim Dyn 45:3461. https://doi.org/10.1007/s00382-015-2550-0

Li S, Lu J, Huang G, Hu K (2008) Tropical Indian Ocean Basin warming and East Asian summer monsoon: a multiple AGCM Study. J Climate 21:6080–6088. https://doi.org/10.1175/2008JCLI2433.1

Liu B, Wu G, Mao J, He J (2013) Genesis of the South Asian high and its impact on the Asian summer monsoon onset. J Clim 26(9):2976–2991. https://doi.org/10.1175/JCLI-D-12-00286.1

Liu G, Wang T, Yang X, Wang Y, Yang X, Cui Y (2017) Climate characteristics of abnormal double-blocking activities over the Ural Mountains and Sea of Okhotsk. J. Meteor. Res. 31(4):694–707. https://doi.org/10.1007/s13351-017-6048-z

Luo JJ, Sasaki W, Masumoto Y (2012) Indian Ocean warming modulates Pacific climate change. Proc Natl Acad Sci USA 109(46):18701–18706. https://doi.org/10.1073/pnas.1210239109

Massachusetts Institute of Technology (2019, May 7). Ocean activity is key controller of summer monsoons: results may help researchers interpret ancient monsoon variations, predict future activity in the face of climate change. ScienceDaily. Retrieved June 3, 2020 from www.sciencedaily.com/releases/2019/05/190507145521.htm. Accessed 3 June 2020

Matsumura S, Sugimoto S, Sato T (2015) Recent intensification of the Western Pacific Subtropical high associated with the East Asian summer monsoon. J Climate 28:2873–2883. https://doi.org/10.1175/JCLI-D-14-00569.1

Matsumura S, Horinouchi T (2016) Pacific Ocean decadal forcing of long-term changes in the western Pacific subtropical high. Sci Rep, 6. https://doi.org/10.1038/srep37765

NASA, accessed in August 2021 at https://podaac.jpl.nasa.gov/forum/

Ning L, Liu J, Wang B (2017) How does the South Asian high influence extreme precipitation over eastern China? J Geophys Res Atmos 122:4281–4298. https://doi.org/10.1002/2016JD026075

NOAA Home News & Features at https://www.noaa.gov/news/2020-was-earth-s-2nd-hottest-year-just-behind-2016. Accessed 30 May 2021

NOAA, Tides and currents https://tidesandcurrents.noaa.gov/sltrends/anomalymapmonth.html, retrieved in March 2019. Accessed 15 Apr 2017

NOAA National Centers for Environmental Information, State of the climate: global climate report for annual 2017, published online January 2018, retrieved on October 1, 2018 from https://www.ncdc.99noaa.gov/sotc/global/201713

NOAA National Centers for Environmental Information: El Niño/Southern Oscillation (ENSO) technical discussion, October Global Release: Tue, 20 Nov 2018

Nützel M, Dameris M, Garny H (2016) Movement, drivers and bimodality of the South Asian high. Atmos Chem Phys 16:14755–14774. https://doi.org/10.5194/acp-16-14755-2016

Pan C, Zhu B, Gao J, Kang H (2017) Source apportionment of atmospheric water over East Asia – a source tracer study in CAM5.1. Geosci. Model Dev. 10:673–688. https://doi.org/10.5194/gmd-10-673-2017

Pervez MS, Henebry GM (2016) Differential heating in the Indian Ocean differentially modulates precipitation in the Ganges and Brahmaputra basins: U.S. geological survey data release. https://doi.org/10.5066/F77P8WH6

Qu X, Huang G (2016) The global warming–induced South Asian high change and its uncertainty. J Climate 29:2259–2273. https://doi.org/10.1175/JCLI-D-15-0638.1

Roxy MK, Ritika K, Terray P, Masson S (2015) Indian Ocean warming—the bigger picture. Bull Am Meteorol Soc (BAMS) 96(7):1070–1071

Roxy MK, Dasgupta P, McPhaden MJ, Suematsu T, Zhang C, Kim D (2019) Twofold expansion of the Indo-Pacific warm pool warps the MJO life cycle. Nature 575(7784):647–651. https://doi.org/10.1038/s41586-019-1764-4

Shimpo A, Takemura K, Wakamatsu S, Togawa H et al (2019) Primary factors behind the heavy rain event of July 2018 and the subsequent heat wave in Japan. Scientific online letters on the atmosphere: SOLA 15A May 2019. https://doi.org/10.2151/sola.15A-003

Sree Raghav R, Mrudula, G (2016) Water vapor transport from the Indian monsoon region: the phenomenon of atmospheric river. In: Proceedings of SPIE - The International Society for Optical Engineering, 3 May 2016, New Delhi

Sun Q, Miao C (2018) Extreme rainfall (R20mm, RX5day) in Yangtze-Huai, China, in June–July 2016: the role of ENSO and anthropogenic climate change. Bull Am Meteorol Soc 99(1):S102–S106. https://doi.org/10.1175/bams-d-17-0091.1

Tollefson J (2016) Global warming already driving increases in rainfall extremes 07 March 2016 Nature. https://doi.org/10.1038/nature.2016.19508

Vinayachandran PN, Shetye SR (1991) The warm pool in the Indian Ocean. Proc Indian Acad Sci (earth Planet Sci) 100:165–175. https://doi.org/10.1007/BF02839431

Wang Y, Wang B, Oh J-H (2001) Impact of the preceding El Niño on the East Asian summer atmosphere circulation. J Meteorol Soc Japan 79(1B):575–588. https://doi.org/10.2151/jmsj.79.575

Wang B, Li J, He Q (2017) Variable and robust East Asian monsoon rainfall response to El Niño over the past 60 years (1957–2016). Adv Atmos Sci 34:1235–1248. https://doi.org/10.1007/s00376-017-7016-3

Wang Q, Li Y, Li Q, Liu Y (2019) Wang YN (2019) Changes in means and extreme events of sea surface temperature in the East China Seas based on satellite data from 1982 to 2017. Atmosphere 10:140

Wang Bin, Xiang Baoqiang, Li Juan, Webster Peter J, Rajeevan Madhavan N, Liu Jian, Ha Kyung-Ja (2015) Rethinking Indian monsoon rainfall prediction in the context of recent global warming. Nat Commun volume 6, Article number: 7154. https://doi.org/10.1038/ncomms8154

Wei W, Zhang R, Wen M, Rong X, Li T (2014) Impact of Indian summer monsoon on the South Asian high and its influence on summer rainfall over China. Clim Dyn 43:1257. https://doi.org/10.1007/s00382-013-1938-y

World Meteorological Organization at https://www.public.wmo.int/en/our-mandate/climate/el-ni%C3%B1ola-ni%C3%B1a-update. Accessed 10 May 2021

Wu R (2002) A mid-latitude Asian circulation anomaly pattern in boreal summer and its connection with the Indian and East Asian summer monsoons. Int J Climatol. 22:1879–1895. https://doi.org/10.1002/joc.845

Xoplaki E, Luterbacher J, Burkard R, Patrikas I, Maheras P (2000) Connection between the large-scale 500 hPa geopotential height fields and precipitation over Greece during wintertime. Climate Res, 14(2), 129–146. Retrieved from http://www.jstor.org/stable/24867280

Zhang J, Tang Q, Chen H, Liu S (2017) Northward shift in circulation system over the Asian mid-latitudes linked to an increasing heating anomaly over the northern Tibetan Plateau during the past two decades. Int J Climatol 37:834–848

Zhang RH, Zheng F, Zhu J and Wang Zhanggui (2013) A successful real-time forecast of the 2010–11 La Niña event. Sci Rep 3, 1108. https://doi.org/10.1038/srep01108

Zhou Z-Q, Xie S-P, Zhang R (2021) Historic Yangtze flooding of 2020 tied to extreme Indian Ocean conditions. Proc Natl Acad Sci 118(12):e2022255118. https://doi.org/10.1073/pnas.2022255118